Rare Metal Materials and Engineering
Volume 50, Issue 10, October 2021
Available online at www.rmme.ac.cn

Science Press

Cite this article as: Jia Zhi, Sun Xuan, Ji Jinjin, et al. Effect of Cold Rolling on the Microstructure and Mechanical Properties of Pure Nickel N6[J]. Rare Metal Materials and Engineering, 2021, 50(10): 3504-3511.

ARTICLE

Effect of Cold Rolling on the Microstructure and Mechanical Properties of Pure Nickel N6

Jia Zhi[1,2], Sun Xuan[2], Ji Jinjin[3], Wang Yanjiang[2], Wei Baolin[2], Yu Lidan[2]

[1] State Key Laboratory of Advanced Processing and Recycling of Nonferrous Metals, Lanzhou University of Technology, Lanzhou 730050, China; [2] School of Material Science and Engineering, Lanzhou University of Technology, Lanzhou 730050, China; [3] School of Materials Engineering, Lanzhou Institute of Technology, Lanzhou 730050, China

Abstract: The effects of cold deformation on the evolution of the microstructure and mechanical properties of pure nickel N6 were investigated. Samples of pure nickel N6 were deformed by cold rolling (CR) to different thickness reductions (20%, 30%, 50%, 70%, 90%). Scanning electron microscopy (SEM), electron backscatter diffraction (EBSD), X-ray diffraction (XRD), microhardness measurements, and tensile tests were used to characterize the microstructure and mechanical properties of the cold-rolled samples. The results show that the grains of pure nickel N6 are refined, and the grain with irregular orientation transforms into a strip-like grain with a preferred orientation parallel to the rolling direction. Micro- and nano-grains of pure nickel N6 are obtained under CR reduction of 90%, at which the grain diameter is mainly below 10 μm, accounting for 94% of the entire grain size. The distribution of low-angle grain boundaries (LAGBs) in the rolled samples is uniform, with a relatively high fraction of misorientation angles of 10° from neighboring points. Upon increasing the cold rolling reductions, the tensile strength and microhardness increase, but the elongation decreases. At a CR thickness reduction of 90%, the tensile strength is 837 MPa, and the microhardness is 2479 MPa, which are 2.32 and 2.7 times higher than those in the unrolled condition, respectively. The fracture morphology of pure nickel N6 at various CR reductions include equiaxed dimples, ridges, and a step morphology, which indicate ductile fracture.

Key words: pure nickel N6; cold rolling (CR); microstructure; mechanical properties; fracture behavior

With excellent mechanical properties, high-temperature resistance, oxidation resistance, and corrosion resistance in concentrated alkali solutions[1,2], pure nickel N6 is widely used in the alkali industry, aerospace, nuclear power and other industrial fields[3]. This material in the form of thin sheets/foils has been recognized as the most suitable material for applications in electrothermal actuators[4], thermocouple sheaths[5], and heat exchangers[6]. However, the relatively poor mechanical properties of pure nickel (tensile yield strength (TYS) of 60 MPa and ultimate tensile strength (UTS) of 320 MPa)[7] should be improved in order to ensure a high reliability in its wide industrial applications. Therefore, some processing routines have been proposed to provide an enhanced strength of pure nickel foils, mainly by refining their grain size. Cold rolling (CR) can be used to produce sheets and strip products that have uniform microstructures and good mechanical performances, with high surface finish, good surface quality, and high production efficiency. However, the production process of sheets and strips is more difficult than that of wire rods. Due to the insufficient understanding of the production process and plastic deformation characteristics of pure nickel sheets and strips, the current production methods of pure nickel products have been unable to meet the production requirements of pure nickel sheets and strips. In addition, some new nickel foil and nickel strip products have appeared on the market which are obtained by the direct cold rolling of raw billets. Compared with the original nickel foil production process, they are produced by cold rolling without the need for remelting, hot forging, and hot rolling. This prevents the introduction of impurities during remelting process, thus improving the purity, and reducing the internal resistance, and ensures

Received date: October 24, 2020
Foundation item: National Natural Science Foundation of China (51665032, 51664041); Science Foundation for Distinguished Young Scholars of Gansu Province (18JR3RA134)
Corresponding author: Jia Zhi, Ph. D., Associate Professor, School of Material Science and Engineering, Lanzhou University of Technology, Lanzhou 730050, P. R. China, E-mail: jiazhi@lut.edu.cn

plasticity. However, this process is used by only a few manufacturers and has seldom been put into large-scale industrial production. Therefore, it is necessary to study the basic theory and cold rolling process related to pure nickel.

Most research on pure nickel has focused on coatings, thermal deformation and corrosion resistance. For example, Genova et al[8] obtained pure nickel coatings by electroless deposition and found that surface morphology has a micro-nano hierarchical structure. Lv et al[9] investigated the effect of electrodeposition temperature on the grain orientation and corrosion resistance of nanocrystalline pure nickel. Wan et al[10] studied the hot deformation behavior and processing workability of a Ni-based alloy. Allart et al[11] researched sulfur grain boundary segregation during the hot deformation of nickel, but there are few studies on the plastic deformation behavior. The cold deformation behavior and mechanical properties of forged pure nickel N6 were studied by Gao et al[1]. The effect of the initial cube texture on the recrystallization texture of cold rolled pure nickel was reported by Chen et al[12]. The mechanical properties and microstructural evolution of pure nickel processed by high pressure torsion (HPT), equal channel angular pressing (ECAP) and deep rolling (DR)[13-16] have been investigated in recent years.

However, there is a lack of available reported data concerning the possible usage of CR method to fabricate high strength nickel sheets and foils. Therefore, the objective of the present study is to investigate the effect of cold rolling on the microstructure and mechanical properties of pure nickel N6 through the analysis of microstructural evolution, mechanical properties, and fracture behavior.

1 Experiment

The experimental material was a forged pure nickel N6 (99.6wt%) slab, whose chemical composition is listed in Table 1. The slab was cut into 40 mm×30 mm×12 mm (length×width×thickness) rolled specimens by a wire electric discharge machine, and the cut samples were polished and ultrasonically cleaned in ethanol. Prior to cold rolling, the pure nickel N6 samples were annealed under vacuum at 973 K for 4 h and cooled in air to room temperature to form a fully recrystallized structure (Fig.3a). Then, the samples were rolled at room temperature with thickness reduction of 20%, 30%, 50%, 70%, and 90%. The cold rolling schedule is listed in Table 2. Each deformation was completed in one pass.

The crystal structure of pure nickel N6 before and after CR deformation was investigated using a D8-ADVANCE X-ray diffractometer, equipped with Cu-Kα radiation (incident wavelength λ was 0.154 06 nm). The tube current was 40 mA, the tube voltage was 40 kV, the 2θ Bragg angle varied from 30° to 90°, and the scanning step was 0.02°.

Table 1 Chemical composition of pure nickel N6 (wt%)

Ni	Cu	Fe	Mn	C	Si	S	Al	Ti
99.6	0.064	0.11	0.05	0.047	0.018	0.045	0.046	0.018

Table 2 Cold rolling schedule of pure nickel N6

Reduction/%	0	20	30	50	70	90
Thickness/mm	12	9.6	8.4	6	3.6	1.2

Microstructure observations were performed on rolled specimens that were cut from cross-section of samples with different cold rolled reductions. The cross-sectional metallographic specimens were ground using sandpapers (from 400# to 3000#). Afterward, the specimens were polished using a 0.5 μm diamond solution and etched in a solution of 3 mL HNO_3+5 mL $C_2H_4O_2$ for 30 s. The metallographic specimens were observed by a FEI Nova NanoSEM 430 scanning electron microscope (SEM). For electron backscatter diffraction (EBSD) analysis, rolled samples were polished by electro polishing in a solution of 90 mL C_2H_5OH and 10 mL $HClO_4$ at −20 °C with a voltage of 50 V. EBSD analysis was performed on a FEI NovaNano SEM 430 equipped with an Oxford Instruments Nordlys 2S detector.

Microhardness measurements were performed using the Vickers hardness tester under a load of 0.05 kg, and the number of measurement on each sample is 9 to create a microhardness polar coordinate nephogram. The illustration of the microhardness test is shown in Fig. 1a, by which each reported hardness value is the average of measurements of 9 times. Tensile tests were performed on the WDW-100D universal testing machine with a strain rate of 0.5 s^{-1}. The size of the tensile sample is shown in Fig. 1b. The fracture morphology of tensile samples was observed by SEM.

2 Results and Discussion

2.1 XRD analysis

Fig.2a shows the XRD patterns of the samples subjected to different reductions in pure nickel N6. The XRD profiles contain three main peaks of (111), (200), and (220). No new peaks or peak offset are generated in the treated samples, which indicate that neither phase transformation, nor any new crystalline phase occur. The diffraction peaks are broadened after cold rolling, and this broadening is intensified upon increasing deformation reductions due to grain refinement and micro-strain after cold rolling[17].

In the XRD patterns, the texture coefficient (T_c) of the pure nickel (*hkl*) crystal plane is used to characterize the preferred orientation level of the pure nickel crystal plane:

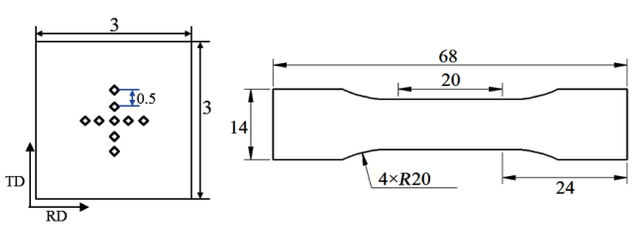

Fig.1 Illustration of the micro-hardness test (a) and size of the tensile test specimen (b)

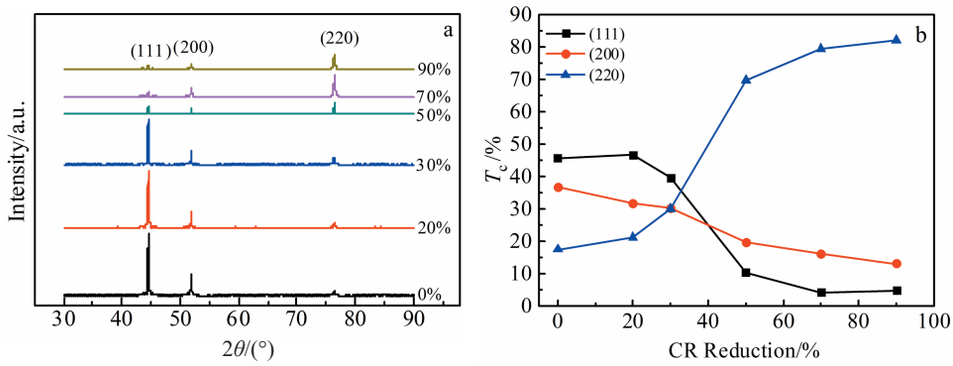

Fig.2 XRD patterns (a) and texture coefficient T_c of each crystal plane (b) of pure nickel N6 under various CR reductions

$$T_c = \frac{I_{(hkl)}/I_{0(hkl)}}{\sum_{i=1}^{n}(I_{(hkl)}/I_{0(hkl)})} \quad (1)$$

where $I_{(hkl)}$ is the measured diffraction intensity, and $I_{0(hkl)}$ is the relative intensity of the nickel (*hkl*) crystal plane without a preferential orientation in the PDF (04-0850) card. The diffraction peak data of each crystal plane of pure nickel with different amounts of deformation and the crystal plane diffraction peak data corresponding to the standard nickel sample were inserted into Eq. (1). The relative diffraction intensity values and T_c results of the six groups are shown in Table 3. Fig. 2b shows T_c of each crystal of pure nickel N6 at various rolling reductions. Increasing the degree of rolling deformation can decrease T_c of both the crystal surface (111) and (200) planes, while the T_c of the (220) plane is increased. When the rolling reduction reaches 90%, the T_c of (220) reaches 82.07%, which indicates that the large CR deformation changes the grain orientation of the original pure nickel N6 structure, and most grains have a (220) plane texture.

2.2 Microstructure observation

Fig. 3 shows the SEM images of pure nickel N6 under different cold rolled reductions (0%, 20%, 30%, 50%, 70% and 90%). Fig. 3a shows the original microstructure of the annealed pure nickel N6, which contains non-uniform grains and has twin structures. Fig. 3b~3f show that the microstructure changes significantly after rolling deformation. As the amount of deformation increases, the grains are significantly refined and begin to gradually flatten and elongate in the direction of the main rolling strain. When the amount of deformation is 70%, an obvious fibrous structure appears.

Table 3 Diffraction intensity and texture coefficient under different reductions

Reduction/%	$I_{(hkl)}$/cps			T_c/%		
	(111)	(200)	(220)	(111)	(200)	(220)
0	70 078	23 663	5 366	45.73	36.76	17.51
20	64 246	18 405	6 147	46.78	31.91	21.31
30	50 015	16 033	7 983	39.63	30.24	30.13
50	8 936	7 115	12 528	10.45	19.80	69.75
70	6 200	9 879	24 160	4.28	16.25	79.47
90	4 711	5 390	16 832	4.8	13.13	82.07

To further explore the effect of cold rolling deformation on the microstructure evolution, EBSD analysis was performed on the samples under 20%, 50%, and 90% deformation. Fig. 4 displays the inverse pole figures (IPFs) and corresponding image quality maps, as well as the distribution of misorientation angles and grain sizes under different CR thickness reductions. The index of the inverse pole figures of selected regions is given in Fig. 4a, in which red is the [001] orientation, green is the [101] orientation, and blue is the [111] orientation. The EBSD map of the 20% cold-rolled pure nickel N6 (Fig. 4a) shows a microstructure that is very similar to the original material, with a relatively large grain size and more twins. The average grain size of 20% cold-rolled pure nickel N6 is 23.7 μm (Fig. 4b). In the grain misorientation angle maps, the high-angle grain boundaries (HAGBs) are >15°, marked by black lines, and the low-angle grain boundaries (LAGBs) are <15°. The green is sub-granular boundaries (SBs, <5°) and the red is Σ3 boundaries. Fig. 4c shows the misorientation angle distributions and the average angle is 17.39°. Furthermore, the fraction of LAGBs is 68.73% and a relatively high fraction (11.7%) of twin boundaries is observed in 20% cold-rolled sample. With further cold-rolling to 50% (Fig. 4d), the grains are gradually elongated along the main rolling direction, and broken fine grains appear. From Fig. 4e and 4f, it can be seen that the grain size and misorientation angle are smaller than those of the 20% rolled specimen. Fig. 4h shows the grain size distribution at a rolling thickness reduction of 90%. It can be seen that most grains have a size below 10 μm, accounting for 94% of the entire grain size and average grain size is 3.864 μm. From Fig. 4g, the grains are severely broken, and the grain boundaries are fuzzy, because the grain boundaries inside the crystals are gradually transformed into LAGBs due to the fracture and rotation of the crystal grains under severe plastic deformation. The fraction of the LAGBs accounts for 81.1% at a rolling thickness reduction of 90% (Fig. 4i).

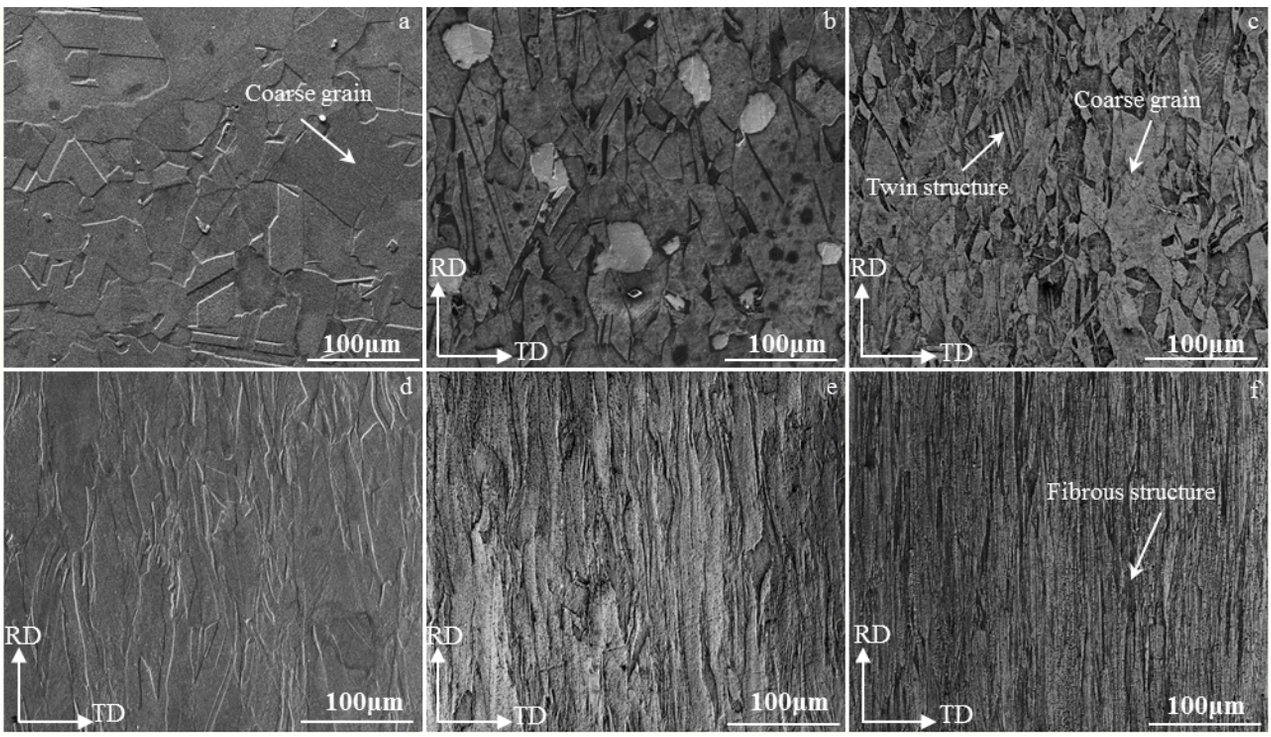

Fig.3 SEM microstructures of pure nickel N6 under various CR deformation reductions: (a) 0%, (b) 20%, (c) 30%, (d) 50%, (e) 70%, and (f) 90%

2.3 Mechanical properties

Fig. 5 shows the microhardness polar coordinate nephogram at various cold rolling reductions. Blue and red represent regions with high and low microhardness values, respectively. In the area of the 9 points measured, the microhardness varies between high and low values, which indicates that the work hardening is uneven due to uneven cold deformation. Metals follow the path of minimum resistance during plastic deformation, which results in uneven deformation. The larger the microhardness, the greater the deformation reduction of the corresponding section. Therefore, the magnitude and distribution of the deformation reduction of different parts are analyzed according to the microhardness value of different parts of the deformed metal. The microstructure after cold rolling shows that the grain size is different, which is one of the reasons for the uneven strain hardening.

The microhardness variation as a function of cold rolling reduction is shown in Fig. 6. The average microhardness of forged pure nickel N6 is 916 MPa, which increases upon increasing the cold rolling reduction. The experimental results reveal that the average microhardness reaches 2479 MPa when the cold rolling reduction is 90%, which is 2.7 times higher than that of as-annealed sample due to the dislocation density variation as a function of the strain hardening due to cold rolling [18]. Strain hardening is attributed to deformation dislocations. During deformation, many dislocation lines pass through the slip surface due to the intersection of slip surfaces, which forms dislocation forests. The movement of dislocations on the slip surface continuously cuts the forest dislocations, resulting in various dislocation tangles, which increase the resistance due to the continual movement of dislocations, resulting in hardening. In addition, the dislocations that cannot move due to the dislocation intersections also cause dislocation accumulation, which also contributes to hardening.

Fig. 7 shows the tensile stress-displacement curves of pure nickel N6 under various cold rolling reductions. The inset shows the fracture of tensile specimens at various cold rolling reductions. The as-annealed pure nickel N6 has excellent plasticity with a displacement of 16.93 mm. It can be seen from the inset in Fig. 4 that the length of the original tensile specimens after fracture is longer than that of other specimens. In addition, the tensile stress-displacement curve of samples with 0% CR reduction has an obvious yield plateau, but the sample with high cold rolling reductions does not.

Fig. 8 shows the mechanical properties of pure nickel N6 under various cold rolling reductions. Upon increasing the deformation reduction, the tensile strength gradually increases. When the deformation reduction is 90%, the tensile strength sharply increases and reaches a maximum of 837 MPa, which is 2.32 times higher than that of original pure nickel N6. However, the elongation rapidly decreases from 50.7% to 5.5% upon increasing the CR reduction to 90%.

There are three main reasons why the tensile strength increases upon increasing CR reduction. Firstly, the grain size decreases upon increasing CR reduction, which contributes to the strengthening. According to the Hall-Petch relationship[19], finer grains lead to higher strength. The improved mechanical

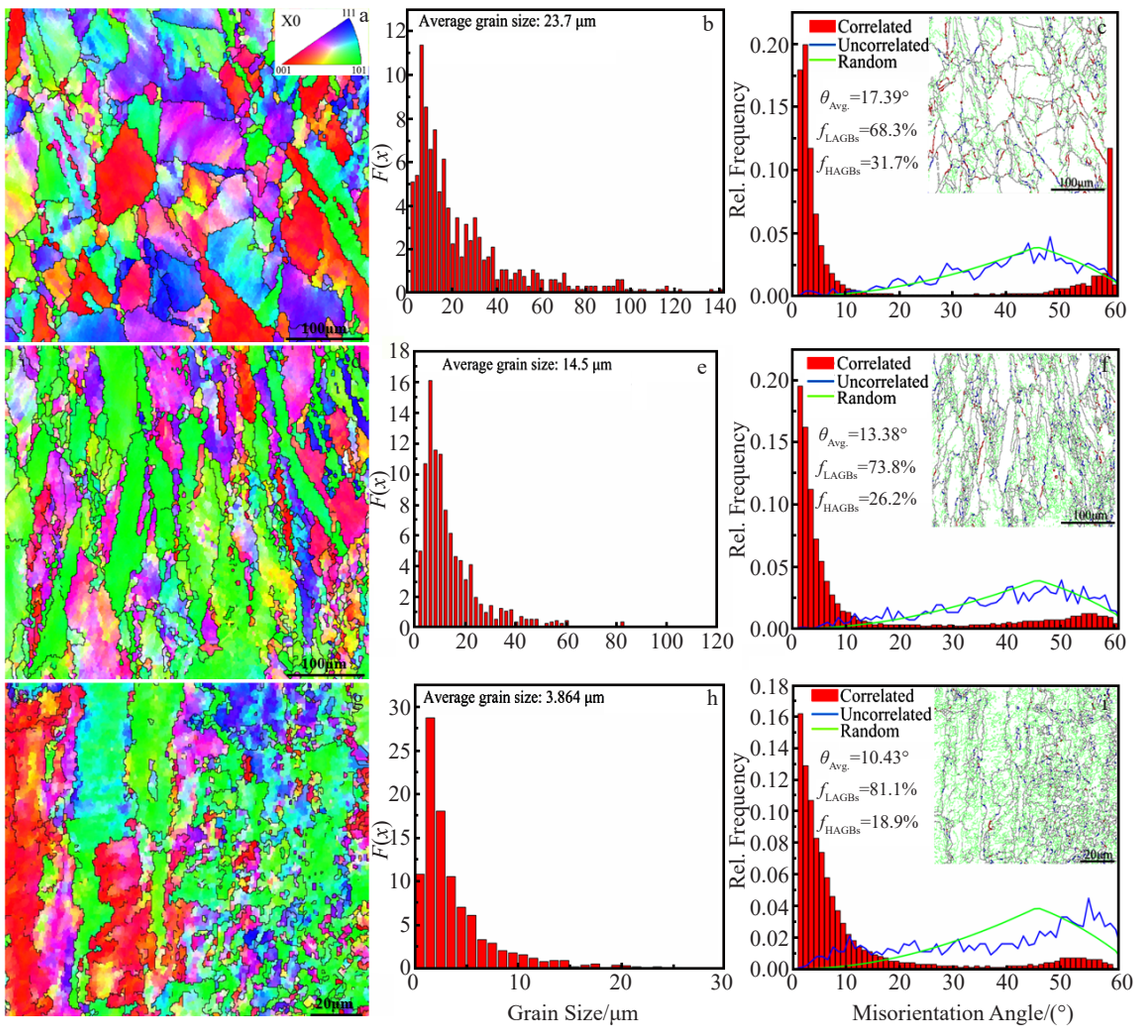

Fig.4 IPF maps (a, d, g), distribution of grain size (b, e, h) and misorientation angle (c, f, i) under different CR reductions: (a~c) 20%, (d~f) 50%, and (g~i) 90%

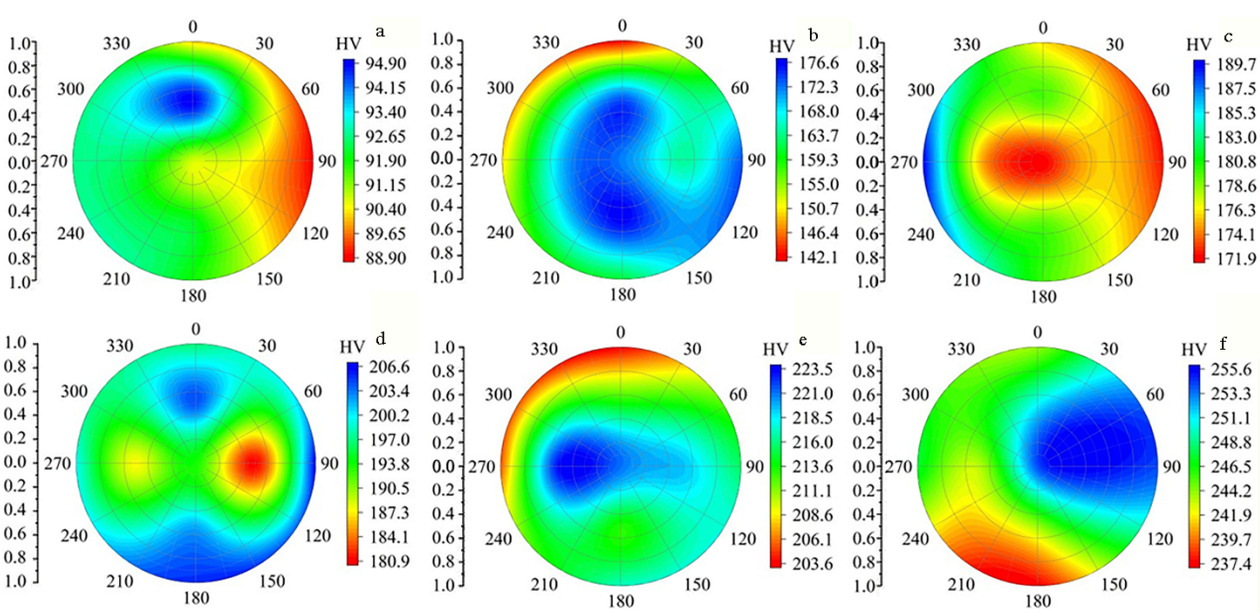

Fig.5 Microhardness polar coordinate nephograms under various cold rolled reductions: (a) 0%, (b) 20%, (c) 30%, (d) 50%, (e) 70%, and (f) 90%

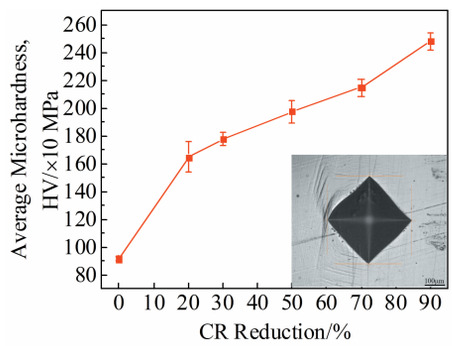

Fig.6 Microhardness of pure nickel N6 nuder various cold rolled reductions (inset shows the microhardness indentation)

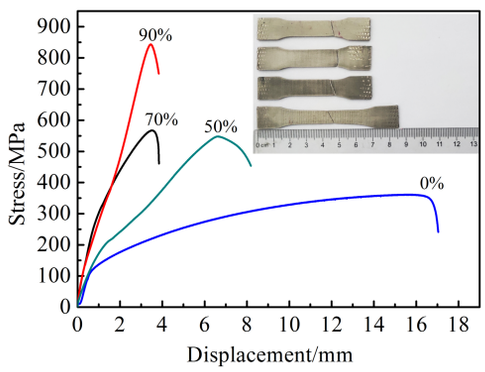

Fig.7 Stress-displacement curves of pure nickel N6 under various cold rolled reductions (inset shows the tensile samples)

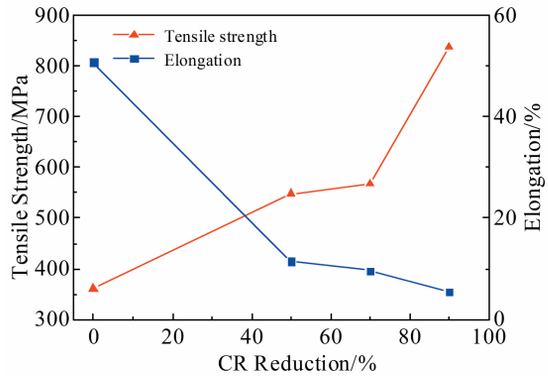

Fig.8 Tensile strength and elongation of pure nickel N6 under various cold rolled reductions

properties due to CR is attributed to the change in the microstructure[20-24]. Secondly, work hardening also plays a significant role in strengthening upon increasing CR reductions, which also leads to increased microhardness (Fig 6). The dislocation density of pure nickel N6 continuously increases, and the interactions between dislocations continuously increase during CR deformation, which restrict dislocation motion, and thus increase the strength. Thirdly, the appearance of texture during CR deformation also contributes to strengthening.

2.4 Tensile fracture

Fig. 9 shows the top view of the fracture surface of N6 under 0% and 90% CR reduction. The fracture plane of the two specimens is about 45° to the tensile direction, which indicates shear fracture (Fig.7 inset). The fractures of the two

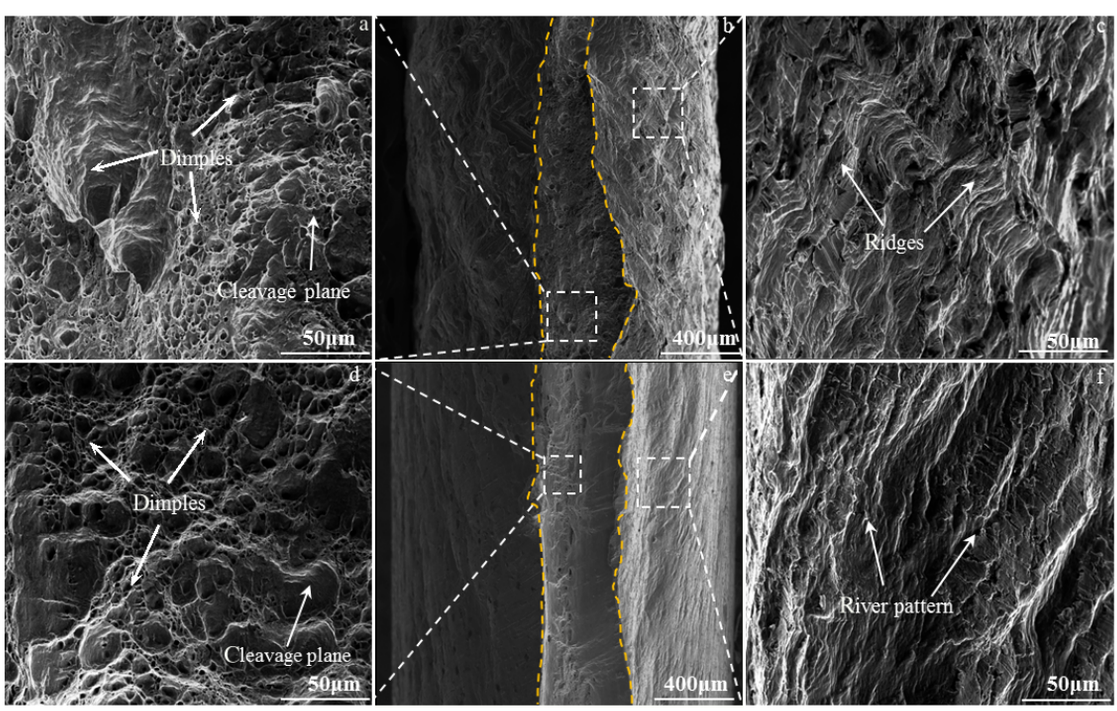

Fig.9 Tensile fracture morphologies of N6 under 0% (a~c) and 90% (d~f) cold rolled reduction

specimens are composed of two parts. The middle part is convex, exhibits an obvious necking phenomenon, and mainly consists of the equiaxed dimples with different sizes and a little bit of cleavage plane. Dimple-rupture ductile fracture[25,26] is observed on the fracture surface (Fig.9a and 9d).

The two sides were shear planes with 45° inclinations, composed of protrusion pattern resembling ridges, the step morphology, and river pattern, which indicate that the fracture mode of the two sample fractures is plastic deformation. In addition, the fractured dimple size and depth of the original sample are larger and deeper than those of sample under 90% CR reduction, which indicates that the plasticity of the original N6 sample is better. The tensile samples under various CR reductions all exhibit different degrees of necking, indicating the ductile fracture of the N6 samples during tensile loading. The necking of the original pure nickel N6 is more pronounced than that of the rolled tensile samples. Compared with specimens before tensile tests, the widths of the original and rolled alloys under 90% reduction are reduced by 23.4% and 4.8%, respectively.

3 Conclusions

1) The grains with random orientation gradually exhibit preferential distribution for pure nickel N6 during the rolling process. Rolled pure nickel changes from the (111) crystal faces to (200) upon increasing the cold-rolling reduction. The grain size of pure nickel N6 under a rolling reduction of 90% reaches the micro and nano level. Under the action of rolling stress, the grain boundaries of pure nickel N6 bear the stress concentration, and the HAGBs gradually change to the LAGBs.

2) Upon increasing the CR reduction, the microhardness and tensile strength of the rolled N6 samples significantly increase due to work hardening, but the elongation decreases. At a thickness reduction of 90%, the tensile strength is 837 MPa, and the microhardness is 2479 MPa, which are 2.32 and 2.7 times higher than those in the unrolled condition; however, the elongation decreases from 50.7% to 5.5%.

3) The specimens exhibit roughly the same tensile fracture morphology which consists of two parts. The middle part is convex and consists of equiaxed dimples with different sizes, and the two sides are shear planes with 45° inclinations composed of ridges and a step morphology. Moreover, the tensile samples at various CR reductions all display different degrees of necking. These two points indicate ductile fracture.

References

1 Gao Zexi, Jia Zhi, Ji Jinjin *et al. Physics and Engineering of Metallic Materials*[J], 2019, 217: 201

2 Gopala Rao Thellaputta, Pulcharu Subhash Chandra, Rao C S P *et al. Materials Today: Proceedings*[J], 2017, 4(2): 3712

3 Palumboa G, Gonzaleza F, Brennenstuhla A M *et al. Nanostructured Materials*[J], 1997, 9(1-8): 737

4 Pimpin Alongkorn, Charoenbunyarit Ittipol, Srituravanich Werayut *et al. Sensors and Actuators A: Physical*[J], 2017, 253: 49

5 Zhong X Y, Wu X Q, Han E H *et al. Engineering Failure Analysis*[J], 2010, 17(6): 1404

6 Harris C, Despa M, Kelly K. *Journal of Microelectromechanical Systems*[J], 2000, 9: 502

7 Polkowski Wojciech, Polkowska Adelajda, Zasadab Dariusz *et al. Materials Characterization*[J], 2017, 130: 173

8 Genova V, Paglia L, Marra F *et al. Surface and Coatings Technology*[J], 2019, 357: 595

9 Lv Jinlong, Liang Tongxiang, Wang Chen *et al. Journal of Solid State Chemistry*[J], 2016, 240: 109

10 Wan Zhipeng, Hu Lianxi, Yu Sun *et al. Journal of Alloy & Compounds*[J], 2018, 769: 367

11 Allart M, Christien F, Gall R Le *et al. Acta Materialia*[J], 2013, 61(20): 7938

12 Chen X P, Chen X, Zhang J P *et al. Materials Science & Engineering A*[J], 2013, 585, 66

13 Neishi K, Horita Z, Langdon T G *et al. Materials Science & Engineering A*[J], 2002, 325: 54

14 Zhilyaev A P, Nurislamova G V, Valiev R Z *et al. Metallurgical and Materials Transactions A*[J], 2002, 33: 1865

15 Zhilyaev A P, Lee S, Nurislamova G V *et al. Scripta Materialia* [J], 2001, 44: 2753

16 Li Xiao, Guan Bo, Jia Yunfei *et al. Acta Metallurgica Sinica*[J], 2019, 32(8): 951

17 Chen Lan, Ren Xudong, Zhou Wangfan *et al. Materials Science & Engineering A*[J], 2018, 728: 20

18 Shabani Ali, Toroghinejad Mohammad Reza, Shafyeia Ali *et al. Materialia*[J], 2018, 1: 175

19 Duan Huiping, Xu Hongxia, Su Wenhuang *et al. International Journal of Minerals, Metallurgy, and Materials*[J], 2012, 19(12): 1128

20 Wang Z, Gao M C, Ma S G *et al. Materials Science & Engineering A*[J], 2015, 645: 163

21 Lian Yong, Huang Jinfeng, Zhang Jin *et al. Materials Science & Engineering A*[J], 2018, 712: 663

22 Li Y, Li J Y, Liu M *et al. Journal of Alloy & Engineering A*[J], 2015, 653: 156

23 Wang Liqiang, Yang Guanjun, Yang Huabin *et al. Rare Metal Materials and Engineering*[J], 2009, 38(4): 579

24 Lan Chunbo, Wu Yu, Guo Lili *et al. Materials Science & Engineering A*[J], 2017, 690: 170

25 Gali A, George E P. *Intermetallics*[J], 2013, 39: 74

26 Guo Junhang, Zhao Shendun, Murakami Ri-ichi *et al. Computational Materials Science*[J], 2013, 71: 115

冷轧对纯镍N6组织和力学性能的影响

贾　智[1,2]，孙　璇[2]，姬金金[3]，汪彦江[2]，魏保林[2]，俞丽丹[2]

(1. 兰州理工大学 有色金属先进加工与循环利用国家重点实验室，甘肃 兰州 730050)

(2. 兰州理工大学 材料科学与工程学院，甘肃 兰州 730050)

(3. 兰州工业学院 材料工程学院，甘肃 兰州 730050)

摘　要：研究了冷变形对纯镍N6组织和力学性能演变的影响。对纯镍N6试样进行了冷轧变形（20%、30%、50%、70%、90%）。采用扫描电子显微镜（SEM）、电子背散射衍射（EBSD）、X射线衍射（XRD）、显微硬度测量和拉伸试验对冷轧试样的组织和力学性能进行了表征。结果表明，纯镍N6的晶粒得到了细化，不规则取向晶粒转变为与轧制方向平行的条状晶粒。纯镍N6在轧制压下量为90%时，晶粒尺寸达到微纳米级别，其中晶粒直径主要在10 μm以下，占全部晶粒尺寸的94%。轧制试样中低角度晶界分布均匀，与相邻点的10°错向角比例较高。随着冷轧压下量的增加，抗拉伸强度和显微硬度升高，伸长率降低。当冷轧程度为90%时，抗拉强度为837 MPa，显微硬度为2479 MPa，分别是退火态的2.32倍和2.7倍。纯镍N6在不同轧制压下量的断口形貌均包括等轴韧窝、棱纹和台阶断口，为韧性断裂。

关键词：纯镍N6；冷轧（CR）；微观组织；力学性能；断裂行为

作者简介：贾　智，男，1985年生，博士，副教授，兰州理工大学有色金属先进加工与循环利用国家重点实验室，甘肃 兰州 730050，E-mail：jiazhi@lut.edu.cn